



ELSEVIER

Available online at www.sciencedirect.com

SCIENCE @ DIRECT®

Experimental Eye Research 79 (2004) 595–612

EXPERIMENTAL
EYE RESEARCH

www.elsevier.com/locate/yexer

Cataract formation in a strain of rats selected for high oxidative stress

Stefania Marsili^a, Rudolf I. Salganik^{b,c}, Craig D. Albright^b, Christopher D. Freel^a,
Sonke Johnsen^d, Robert L. Peiffer^e, M. Joseph Costello^{a,*}

^aDepartment of Cell and Developmental Biology, School of Medicine, University of North Carolina at Chapel Hill, Chapel Hill, NC 27599, USA

^bDepartment of Nutrition, School of Public Health, University of North Carolina at Chapel Hill, Chapel Hill, NC 27599, USA

^cInstitute of Cytology and Genetics, Russian Academy of Sciences, Siberian Division, Novosibirsk 630090, Russian Federation

^dDepartment of Biology, Duke University, Durham, NC 27708, USA

^eMerck Research Laboratories, P.O. Box WP45-226, West Point, PA 19186, USA

Received 5 December 2003; accepted 7 June 2004

Available online 30 July 2004

Abstract

The primary purpose of this study was to define the clinical and morphological features of cataractogenesis in the OXYS strain of rats that generate excess reactive oxygen species. Rats were sequentially examined from birth to the development of mature cataracts with slit lamp biomicroscopy. Morphology of selected stages of cataract development was studied using light and transmission electron microscopy (TEM), immunohistochemical localization of the lipid peroxidation product 4-hydroxynonenal (HNE) and fluorescent antibody labeling for DNA oxidation products. Lenses from age-matched normal rats were used as controls.

OXYS rats developed cataracts as young as two weeks of age with progression to maturity by 1 year. Clinically, cataracts appeared initially either as nuclear or sub-capsular cortical changes and progressed to pronounced nuclear cataracts within months. TEM confirmed the light microscopic impression of region-specific alterations in both fiber cell cytoplasmic protein matrix and membrane structure. The outer adult nuclear region showed extensive cellular damage similar to osmotic cataracts, which is consistent with the postulated high uptake of glucose in the OXYS strain. The adult and outer fetal nuclear cells displayed several types of focal damage. The inner fetal and embryonic nuclear cells demonstrated textured cytoplasm, suggesting protein degradation or redistribution. Staining for HNE was increased in epithelium, cortex and nucleus compared to control lenses. Fluorescent antibody probes demonstrated increased levels of DNA oxidation products in OXYS rat lenses compared to age-matched controls. Fourier analysis of nuclear cytoplasm revealed significant components with corresponding sizes greater than 100 nm and, using a new theoretical approach, the texturing of the cytoplasm was shown to be sufficient to cause opacification of the nucleus. The OXYS rat appears to be an ideal model for oxidative stress cataractogenesis. The potential oxidative damage observed is extensive and characteristic of the developmental region. The source of oxidative damage may in part be a response to elevated levels of glucose. Because oxidative stress is thought to be a major factor in cataract formation in both diabetic and non-diabetic aging humans, this animal model may be a useful tool in assessing efficacy of antioxidant treatments that may slow or prevent cataract formation.

© 2004 Elsevier Ltd. All rights reserved.

Keywords: oxidative stress; cataract; rat model; light microscopy; electron microscopy; immunohistochemistry; lens fiber cell; Fourier analysis

1. Introduction

Age-related cataract remains a major cause of blindness, affecting over 20 million of the nearly 45 million blind people worldwide with the highest incidence occurring in developing countries (Thylefors, 1995, 1999; Nirmalan et al., 2003).

Presently, surgery is the only approach for the treatment of cataract, and while favorable outcomes are quite predictable, the limited number of surgeons in underdeveloped countries and the high cost of surgery have made cataract a major public health problem (Minassian and Mehra, 1990; Whitfield et al., 1990; Pokharel et al., 1998). Drugs developed to delay or prevent lens opacification have failed to give convincing positive results in clinical trials (Harding, 2001). Although there has been significant progress in understanding the sources of scattering in many types of human cataract, the mechanisms that explain cataract formation in

* Corresponding author. Dr M. Joseph Costello, Department of Cell and Developmental Biology, School of Medicine, University of North Carolina at Chapel Hill, Chapel Hill, NC 27599-7090, USA.

E-mail address: mjc@med.unc.edu (M. Joseph Costello).

the most common type, nuclear age-related cataract, are uncertain and are under intense investigation.

Oxidative stress has been identified as one of the major causes of age-related diseases, including cardiovascular diseases, arthritis, brain dysfunction, emphysema and cataract (Ames et al., 1993; Salganik et al., 1994a–d; Salganik, 2001). Generation of reactive oxygen species (ROS), resulting in degradation, crosslinking and aggregation of lens proteins, is regarded as an important factor in cataractogenesis (Spector, 1984; Taylor and Nowell, 1997; Truscott, 2000). Lipid peroxidation due to oxidative stress occurs in human cataract and lens opacity has been found to correlate with the level of LPO degradation products accumulated in the lens (Babizhayev et al., 1988). LPO is implicated in human cataractogenesis because the toxic peroxidation products induce fragmentation of soluble lens proteins and damage vital membrane structures, correlating with an increase in lens opacity and changes in the refractive properties of the lens (Bhuyan et al., 1986; Babizhaev et al., 1987; Awasthi et al., 1996). It is known that lipid peroxides undergo degradation to form toxic reactive aldehydes, such as HNE. Rat lenses cultured in the presence of HNE and high glucose levels developed cataractous changes (Ansari et al., 1996). In humans the level of reactive aldehydes was higher in well-developed cataractous lenses compared to normal lenses (Bhuyan et al., 1986). Interestingly, it has been recently reported that HNE can mediate oxidative stress-induced cell death in many cell types including lens epithelial cells (Choudhary et al., 2002). DNA is also a target of increased oxidative stress, which has been shown to induce DNA damage and apoptosis in the epithelial cells in the human cataractous lenses (Imlay and Linn, 1988; Spector, 1995). Studies in rat lens in vitro suggest that the induction of apoptotic DNA fragmentation in lens epithelial cells could initiate lens opacification (Li et al., 1995).

Development of cataracts is also associated with the accumulation of sugar metabolites within the lens and glycation of proteins (Monnier, 1990; Swamy-Mruthinti et al., 1999). Autoxidation of sugars is regarded as a source of ROS (Thornalley et al., 1984; Wolff and Dean, 1987). The excess of ROS, together with glycation of proteins, are very likely to be major causes of lens damage and light scattering.

In order to investigate the aging process and cataract formation, different approaches have been used to create suitable animal models of cataractogenesis (Tripathi et al., 1991). Emory mouse (Kuck, 1990), Philly mouse (Kador et al., 1980), senescence-accelerated mouse (Hosokawa et al., 1984) and SRC rat (Okano et al., 1993) are examples in which acceleration of certain aging parameters and biochemical markers mimic some changes observed in aging human lenses. However, none of the animal models develops cataracts similar to those seen in humans. A more appropriate animal model of human age-related nuclear cataract is needed.

The OXYS strain of rat, selected for high oxidative stress, appears to be such an animal model capable of reproducing many of the key features of human age-related cataracts. This animal model shows premature aging and significantly shortened life span associated with oxidative damage to a variety of tissues and organs due to inherent overgeneration of ROS (Salganik et al., 1994a–d; Yelinova et al., 1996; Men'shchikova et al., 2002; Ishchenko et al., 2003). Many changes in OXYS lens fiber cells, characteristic of specific developmental regions, mimic the development of age-related cataracts in humans. Previous studies support the hypothesis that the early onset of increased light scattering, indicative of lens damage, is most likely due to inherited changes in cellular properties linked to elevated glucose uptake and metabolism in the lens (Solovyova et al., 1987; Salganik et al., 1994c). The aim of this study is to provide preliminary characterizations of selected biochemical and morphological features of cataract formation to determine the validity of the OXYS rat as model for human cataractogenesis. Biomicroscopic examination of the cataract progression, histochemical evidence that DNA and lipid oxidation products are significant and ultrastructural analysis of extensive morphological changes observed in the OXYS rat lenses support the hypothesis that the OXYS rat represents a valuable model for human age-related cataract formation. Particularly relevant is presentation of a new theoretical treatment using Fourier analysis to show that the textured cytoplasm (due to the modification and redistribution of fiber cell proteins) is sufficient to account for the observed opacification of the lens nucleus. Portions of this work have been presented previously (Marsili et al., 2000; Costello et al., 2000).

2. Materials and methods

2.1. Animals

The OXYS strain of rats evolved from the attempts to develop a rat strain with inherited galactosemia (Salganik and Solovyova, 1972; Solovyova et al., 1975; Salganik, 1979). To attain this goal, young Wistar rats were fed galactose-rich diets and animals highly susceptible to the cataractogenic effect of this diet were selected for inbreeding. After five cycles of inbreeding, feeding galactose-rich diet and selection, the following generations of rats developed cataracts spontaneously without galactose in the diet. Development of cataracts and low levels of galactose-1-phosphate uridylyltransferase, characteristic of humans with inherited galactosemia, allowed these animals to be regarded as a galactosemic rat strain. Thereby, the W/SSM rat strain was developed (Solovyova and Salganik, 1982). However, it was established that an enhanced transport of glucose into the cells of OXYS rats, rather than low galactose-1-phosphate uridylyltransferase activity, is the characteristic inherited feature of these

animals (Salganik et al., 1994a,c). Genetic analysis has shown that this feature is ensured by a single dominant gene that appears to be responsible for the up regulated glucose uptake (Solovyova et al., 1987). However, the animals are not diabetic and have normal levels of blood glucose (Solovyova et al., 1987). This genetic pattern, associated with a mutation in hexose transport mechanism, is reproduced obviously in all cells of the animals including lens cells. Accumulation of glucose and other hexoses within cells led to overgeneration of ROS most probably through the well-established process of autoxidation of sugars (Wolff, 1994). Oxidative damage of mitochondria membranes decreased oxidative phosphorylation and increased membrane permeability that resulted in additional ROS generation (Salganik et al., 1994d; Men'shchikova et al., 2002). Low levels of superoxide dismutase and catalase could also contribute to accumulation of ROS (Yelinova et al., 1996). In turn, an increase in formation of oxidized thiols is associated with enhanced generation of ROS (Yelinova et al., 1996). High levels of ROS in cells of these animals led to the oxidation of proteins, lipids, DNA rearrangements, to the impairment of cell structures and to the development of cataracts. This rat strain was renamed by the International Rat Genetic Nomenclature Committee as the OXYS rat strain and the normal control inbred rats as the OXYR strain. The strains were imported by one of us (RIS) from the Institute of Cytology and Genetics (Novosibirsk, Russia) and the colony was maintained here for use in this and other studies (Albright et al., 1998). Shortly after the current preliminary studies were completed, the colony showed anomalous loss of characteristic features perhaps due to the inherent difficulty in breeding or unpredicted beneficial mutations. A limited number of OXYS rats were available for this study and attempts to reestablish the colony have not been successful. The original colony in Russia remains viable and the subject of recent studies (Kolossova et al., 2001; Men'shchikova et al., 2002; Ishchenko et al., 2003).

All animals were fed standard AIN-93M diet (Dyets, Inc., Bethlehem, PA) without additives and given water freely. A total of 24 OXYS rats were used for different parts of this study. Animals used in this study were treated in accordance with the ARVO Statement on the Use of Animals in Ophthalmic and Vision Research, and the research protocol was reviewed and approved by the University of North Carolina Institutional Animal Care and Use Committee.

2.2. Clinical examination

Clinical examinations of OXYR and OXYS rats under sedation were performed every two weeks starting at 2 weeks of age up to 6–12 months of age. Following dilation of the pupil with topical 1.0% tropicamide, the anterior segment of the eye was examined with a biomicroscope and the posterior segment with an indirect

ophthalmoscope. Observations were made on 20 animals (6 OXYR and 14 OXYS) over 1–12 months. Lens morphology was documented descriptively and by slit-lamp photography. Age-matched pairs of OXYS rats with cataracts and OXYR controls were sacrificed at 1, 3 and 6 months with CO₂ asphyxiation. Enucleation was performed immediately post-mortem and lenses were rapidly fixed for further analysis.

2.3. Light microscopy and immunohistochemical analysis

Longitudinal analysis of lens changes comparing age-matched controls and OXYS rats was performed. Fiber cell morphology of selected stages of cataract development was studied using light microscopy. Histological sections (6–10 μ m) were prepared from formalin-fixed, paraffin embedded OXYR ($n = 6$) and OXYS ($n = 6$) rat eyes and mounted on glass slides. Mounted sections were either stained with hematoxylin and eosin (H and E) or Periodic Acid-Schiff (PAS) reaction, or processed for immunohistochemistry to determine the distribution and extent of LPO and DNA oxidation. A monoclonal antibody against HNE (Oxis Pharma, Portland, OR), a toxic reactive aldehyde product of LPO (Baldwin et al., 1998), was used to probe histological sections from control and OXYS lenses. The intensity of HNE brown immunocytochemical reaction product generated was determined by measuring the optical density with reference to a standard curve obtained from a calibration gray-scale wedge filter (Kodak T-14 calibrated gray-scale) and NIH Image software (Albright et al., 1999). Markers of oxidative damage to DNA were detected by a monoclonal antibody (QED Biosciences, San Diego, CA) that recognizes 8-hydroxy-2'-guanosine, 8-hydroxyguanine, and 8-hydroxydeoxyguanosine in cells (Al-Abdulla and Martin, 1998). Oxidative DNA damage was confirmed using avidin-FITC (Struthers et al., 1998).

2.4. Transmission electron microscopy

For electron microscopy, OXYR ($n = 4$) and OXYS ($n = 4$) lenses were sectioned fresh with a Vibratome and the 200 μ m thick slices were immersion fixed for 12–18 hr in 2.5% glutaraldehyde, 2% paraformaldehyde and 1% tannic acid in 0.1 M cacodylate buffer at pH 7.2. Post-fixation was done in 0.5% osmium tetroxide for 1 hr at 4°C and uranyl acetate at room temperature, followed by ethanol dehydration and embedding in epon. The Vibratome slice containing the optic axis was bisected to expose the fiber cells in cross-section in the equatorial plane (Freel et al., 2002). Mesas were raised to cut 60–90 nm thin sections that were supported on copper grids, stained with uranyl acetate and lead citrate and examined at 80 kV with a FEI-Philips Tecnai 12 (Hillsboro, OR) transmission electron microscope (Freel et al., 2002).

2.5. Image analysis

2.5.1. Fourier analysis of cytoplasmic texture

Our methods for quantitatively characterizing cytoplasmic texture using Fourier analysis techniques have been documented in several recent publications (Taylor et al., 1997; Taylor and Costello, 1999; Freel et al., 2002, 2003). In brief, high-magnification micrographs of fiber cell cytoplasm (21 000 ×) were collected digitally and Fourier analysed using Gatan's Digital Micrograph image processing software (v.3-4, Gatan Inc., Pleasanton, CA). Surface plots of these transforms were constructed in MATLAB (v.5, The MathWorks, Inc., Natick, MA). Radially averaged plots were generated by circularly averaging the Fourier transform data as a function of its radius (NIH Image, v.1-62, US National Institutes of Health, <http://rsb.info.nih.gov/nih-image/>). Radial plot coordinate data from multiple specimens within each group were combined to produce averaged curves using Microsoft Excel (v. 2000, Microsoft Corporation, Redmond, WA). Subtracting the averaged data of a smooth or slightly textured specimen group from that of a more textured group produced the difference curves.

2.5.2. Fourier theory of light scattering and opacity

The distribution and intensity of light scattered by a thin section of biological tissue is closely related to the Fourier transform of the spatial variation of the section's complex refractive index (reviewed by Lipson, 1972; Hecht, 1998). The complex index is $n + ih$, where n is the refractive index and h is proportional to the absorption coefficient. However, because biological molecules in general do not absorb significantly at visible wavelengths (reviewed by Johnsen, 2001), h is set to zero in this study. The Fourier transform of the tissue section is then given by

$$F(k_x, k_y) = \mathfrak{F}\{n(x, y)\} = \int_{-\infty}^{+\infty} \int_{-\infty}^{+\infty} n(x, y) \cdot e^{i(k_x x + k_y y)} dx dy \quad (1)$$

where $\mathfrak{F}\{\}$ is the transform, k_x and k_y are the horizontal and vertical components of the spatial frequencies, and $n(x, y)$ is the real refractive index of the tissue. The spectral power of the refractive index variations as a function of the frequency magnitude $\nu = \sqrt{k_x^2 + k_y^2}$ is

$$P(\nu) = \sum_{\nu = \sqrt{k_x^2 + k_y^2}} F(k_x, k_y) \cdot F^*(k_x, k_y) \quad (2)$$

where F^* is the complex conjugate of F . This spectral power is related to the light scattered by the section by

$$I(\theta) = P\left(\frac{\bar{n}L \sin \theta}{\lambda}\right) \quad (3)$$

where $I(\theta)$ is the intensity of light scattered into angle θ , λ is the wavelength of the incident light, and \bar{n} and L are the average refractive index and diameter of the section, respectively (Hecht, 1998). The total amount of light scattered is the integral of $I(\theta)$ over all possible angles.

Due to the small thickness of the section (less than 100 nm), no significant light was scattered at angles greater than 90°. Thus:

$$S = \int_0^{\pi/2} I(\theta) d\theta. \quad (4)$$

Therefore, given the refractive index distribution of the tissue section and the wavelength of the incident light, one can determine the amount of light scattered into various angles by the section. However, a tissue section that scatters a large amount of light at high angles may be more opaque than a section that scatters a small amount of light at very low angles. This concept is formalized by calculating what is known as the asymmetry parameter g (Bohren, 1987). This parameter is the average cosine of the scattered light and is given by:

$$g = \langle \cos \theta \rangle = \frac{1}{S} \int_0^{\pi/2} I(\theta) \cos \theta d\theta. \quad (5)$$

Most studies of light scattering in complex materials use the following product:

$$\sigma = S \cdot (1 - g) \quad (6)$$

This product accounts for both the amount of light scattering and the degree to which the scattering deflects the incident light (Bohren, 1987). Objects that scatter light over small angles have a high g and therefore a low σ . Objects that scatter light at 90° have a g of 0 and therefore a high σ . This product, known variously as 'hiding power' (by the commercial paint industry), 'angle-weighted scattering coefficient', or 'reduced scattering coefficient', is the best available predictor of the opacity of an object. For this reason, σ will be referred to hereafter as opacity.

2.5.3. Two-dimensional Fourier analysis of sections

In biological tissue, refractive index is linearly proportional to density and relatively independent of the actual molecule (Michielsen, 1999). In addition, the heavy metal stains used in electron microscopy are generally non-specific, particularly for proteins but not for membranes (Glauert, 1965; Hayat, 1971). For these two reasons, EM staining intensity has been used as an indicator of refractive index by many researchers (Gisselberg et al., 1991; Vaezy and Clark, 1994; Vaezy and Clark, 1995; Vaezy et al., 1995; Taylor et al., 1997; Prum et al., 1998; 1999a,b; Taylor and Costello, 1999; Clark, 2001). Although the relationship between the density of metal stain and refractive index is not perfect, it is used in this study because it is the best available. Indeed, at optical wavelengths the refractive index can only be directly measured using optical techniques, which have a resolution limit of approximately half the wavelength of light used; therefore, calculations based on an assumed density/index relationship is a suitable

method for determining the refractive index at electron microscopy resolution.

First, a 1024×1024 pixel region of interest was selected from a representative electron micrograph. The refractive index of white pixels was set equal to that of cytoplasm, 1.35 (Charney and Brackett, 1961). The refractive index of black areas was set to be that of dense protein, 1.55 (Freegard, 1997). The region of interest was then multiplied by a Hanning window function that reduces the amplitude of the spatial variation of the index as it approaches the edge of the region of interest. This is done because the Fourier transform assumes that the region of interest wraps around at all edges (i.e., is a torus) and thus gives spurious frequencies due to the sharp discontinuities at the edges. The windowed ROI was then Fourier-transformed using the Fast Fourier Transform algorithm. The transform was then multiplied by its complex conjugate to create a two-dimensional power spectrum (with the zero order at the center of the transform).

Because the Fast Fourier Transform is a discrete transform of a discretely sampled image, the remainder of the algorithm differs slightly from the general theoretical treatment given in Section 2.5.2. The total power at a given spatial frequency was calculated by binning the transform into bins centered on integral frequencies (i.e., 1, 2, 3...) and summing within each bin. The zero order was ignored because it has no effect on the opacity (see Eq. (6)). The first order was also ignored because the envelope of the Hanning window contributes a large Fourier amplitude at this frequency. The scattering angle for each integral spatial frequency was determined by solving Eq. (3) for θ :

$$\theta = \sin^{-1}\left(\frac{\lambda\nu}{\bar{n}L}\right). \quad (7)$$

The total scattering S was then calculated by summing the spectral power at each spatial frequency that was associated with a scattering angle less than or equal to 90° :

$$S = \sum_{\sin^{-1}(\lambda\nu/\bar{n}L) \leq \pi/2} P(\nu). \quad (8)$$

The asymmetry parameter g was calculated by including $\cos \theta$ in Eq. (8):

$$g = \frac{1}{S} \sum_{\sin^{-1}(\lambda\nu/\bar{n}L) \leq \pi/2} P(\nu) \cos \theta. \quad (9)$$

The opacity was then calculated using Eq. (6).

3. Results

The photograph of representative OXYR and OXYS rats at 3 months of age clearly displays the mature bilateral cataracts in the OXYS rat (Fig. 1(A)). The OXYS rats are smaller and usually fully blind by adulthood from spontaneous cataracts. Clinical biomicroscopic examination

of OXYS rats at different ages yields some distinctive features of their cataractous lenses (Fig. 1(B)–(D)). Although opacification was observed to begin in several locations, increased scattering often began near the cortex/nucleus interface (Fig. 1(B), arrow) or just outside the fetal nucleus (Fig. 1(C), arrow), and is usually evident at 1–2 months of age. Total nuclear opacification with progressive cortical involvement occurs through 6–12 months of age (Fig. 1(D)). The equatorial cortex often displays vacuoles (Fig. 1(D), arrow) indicating possible osmotic stress. Nearly all of the OXYS rats had mature cataracts by 6 months; very few OXYR rats showed any form of lens scattering and none had mature cataracts.

Fluorescent labels attached to monoclonal antibodies that bind DNA fragments produced by oxidative damage show intense labeling in the 3-month-old adult OXYS rat epithelium compared to the age-matched OXYR control (Fig. 2(B) and (A), respectively). The label also highlights the hypertrophy and hyperplasia of the OXYS epithelium (Fig. 2(B), arrow). The hyperplasia and spindle metaplasia are emphasized in H and E stained OXYS histological sections (Fig. 2(C) and (D)) where the capsule is tightly adherent and the underlying cortex appears to have separated from the epithelium during the sample preparation. These histological features are frequently associated with anterior subcapsular cataract, although not necessarily with diabetic cataract (Font and Brownstein, 1974). PAS stain (Fig. 2(E) and (F)) demonstrates the ectopic production of the basement membrane in a region of epithelial hyperplasia (Fig. 2(E), arrow) and swollen fiber cells in the posterior equatorial cortex are evident just beneath the lens capsule (Fig. 2(F), arrows).

Pronounced high levels of LPO are indicated in immunohistochemical staining of HNE reaction product from 1-month-old OXYS rats (Fig. 3). Note that the reaction product outlines the capsule (Fig. 3(A) and (B)) and highlights the nuclei of the epithelium and bow region of the OXYS lens (Fig. 3(B)). The fiber cell interfaces are well defined by the brown reaction product suggesting a preferential deposition at plasma membranes. Note the absence of fiber cell swelling and osmotic stress in this young lens. The entire nucleus of the OXYS shows a high-level reaction product (Fig. 3(C) and (D)), which is significantly higher than the OXYR lenses based on calibrated optical density measurements (Fig. 4).

TEM images of normal transparent OXYR control lenses (Fig. 5) display the typical pattern of fiber cells (Freel et al., 2003). The outer cortex shows large newly formed fiber cells in cross-section having a flattened hexagonal shape (Fig. 5(A)). Fiber cells of the adult nuclear region in these 6-month-old OXYR lenses are slightly more irregular in shape, although the hexagonal shape and packing in radial cell columns are still recognizable features (Fig. 5(B)). Often, circular profiles bounded by paired membranes are present within the cytoplasm (Fig. 5(B), arrow). These profiles are most likely cross and oblique sections

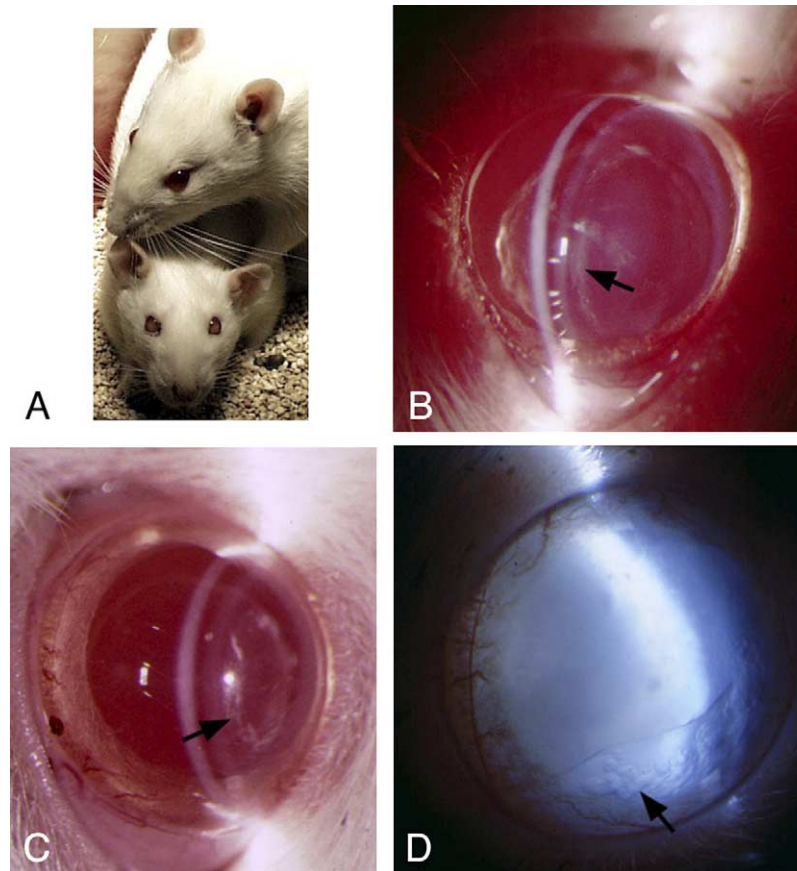


Fig. 1. (A) Photograph of 3-month-old OXYR (top) and OXYS rats depicting the large size of the former and the obvious cataracts in the latter. (B and C). Early nuclear opacities in 1-5-month-old OXYS rats. The zone of initial opacification (arrows) is often the nuclear layer between the fetal nucleus and the cortex. (D). Advanced nuclear and cortical cataract visible in a 6-month-old OXYS rat. Note the inferior equatorial vacuoles (arrow).

of finger-like projections derived from the cellular interdigitations rather than isolated cytoplasmic vesicles (Gilliland et al., 2001). The nucleus of the lens displays irregular fiber cells that have large cross-sections and are not regularly packed in radial cell columns, a typical finding of the primary and early secondary fiber cells of mammalian lenses (Taylor et al., 1996; Al-Ghoul and Costello, 1997). In all regions, the OXYR fiber cells display smooth homogeneous cytoplasm without cell damage or disruption. In contrast, the 6-month-old OXYS rat lenses contain damaged cells in all regions. Four distinct types of cell damage are illustrated in Fig. 6. Fiber cells of the outer cortex are enlarged and irregular in shape probably due to osmotic swelling (Fig. 6(A)). Fiber cells at the cortical/nuclear interface display a wide variety of severe damage including vesicles, globules, distortion of cell shape and accumulation of densely staining cytoplasmic material (Fig. 6(B)). The fetal nuclear region shows a distinctive type of cell disruption in which membranes aggregate into multilamellar swirls within globular structures (Fig. 6(C), arrow). Very similar multilamellar bodies were recently described in human nuclear cataract (Gilliland et al., 2001). The fiber cells of the inner fetal and embryonic nuclei display an unusual type of damage of the cytoplasmic

protein matrix in which numerous small spots of low density are present in an otherwise homogeneous background (Fig. 6(D)). The texture of the OXYS nuclear cytoplasm is similar to that reported for the fiber cells in the opaque nucleus of the diabetic canine lens (Taylor et al., 1997).

A more subtle type of cellular damage occurs in the OXYS outer cortex fibers that appear to form extensive sites of fusion (Fig. 7). In a narrow 50 μm band about 100 μm from the lens surface (Fig. 7(A)), adjacent fiber cells display numerous fusion sites that are characterized by 0.1–0.5 μm diameter openings (Fig. 7(B), arrows) bordered by continuous loops of plasma membrane (Fig. 7(C), box). Also frequently present are lens junctions with the typical pentalamellar structure and no visible extracellular space (Fig. 7(D), arrowhead). An equivalent region was not evident in OXYR lenses.

A unique type of fiber cell damage in the OXYS adult nucleus was observed in a narrow 50–100 μm band 420 μm from the lens surface (Fig. 8). This distance is known accurately because individual thin sections of the equatorial plane extended from the lens surface to the embryonic nucleus. A low magnification montage of the entire thin section located the critical region within the adult nucleus (Fig. 8(A)). This region displayed occasional globular

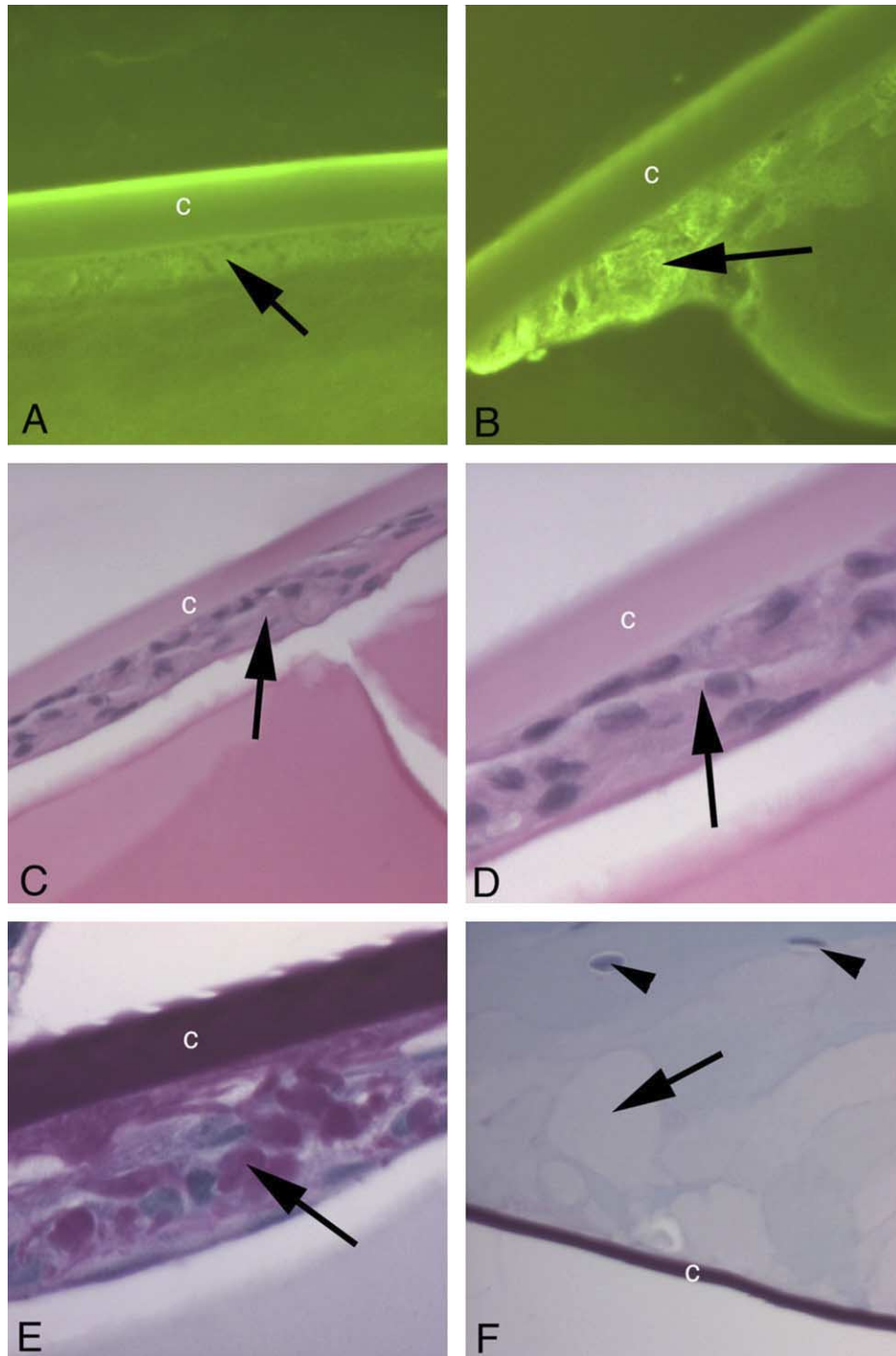


Fig. 2. Light microscopic images of lenses near the capsule (denoted by 'c') in 3-month-old rats. (A). Fluorescent antibody probe of DNA oxidation in OXYR rat lens demonstrates weak labeling of the epithelium (arrow), $400\times$. (B). Fluorescent antibody image of an OXYS rat lens shows intense positive response of the epithelium (arrow), $400\times$. (C and D). Cataractous changes in the epithelium (arrows) in an OXYS rat consisted of hypertrophy, hyperplasia and spindle metaplasia of the lens epithelium. Hematoxylin and eosin. C, $200\times$ and D, $400\times$. (E). Periodic Acid-Schiff stain demonstrates ectopic production of basement membrane-like material by the hyperplastic epithelium (arrow), $400\times$. (F). The equatorial posterior cortex was characterized by swollen lens fibers (arrow) beneath a thin capsule. Nuclei of the peripheral lens bow are seen within the posterior cortex (arrowheads), $100\times$.

disruptions (Fig. 8(A), red arrowhead), but otherwise the fiber cells (which are not readily visible at this magnification and contrast) on either side of the disrupted region were hexagonal in shape and packed in radial cell columns similar to the cells in the OXYR (Fig. 6(B)). Within the thin band of

the adult nucleus (Fig. 8(A), between the arrows), the cytoplasm of many of the fiber cells contained a unique fibrillar pattern (Fig. 8(B)–(D)). The cells with the fibrillar pattern of disruption were observed adjacent to each other and to cells with normal appearing cytoplasm separated by

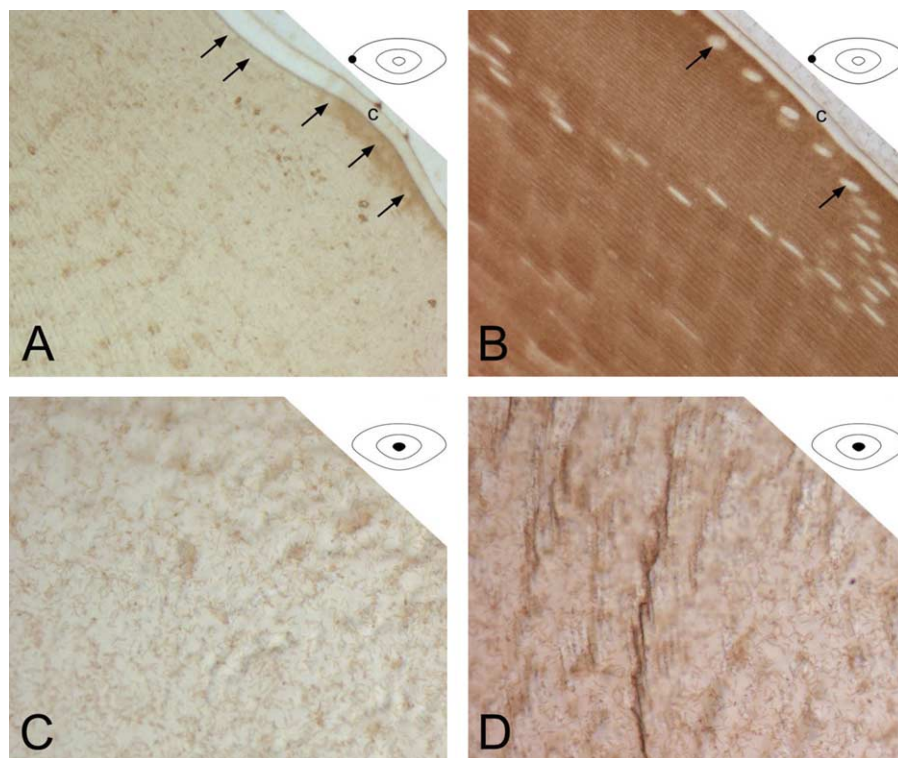


Fig. 3. Immunohistochemical localization of 4-hydroxynonenal (HNE) in 1-month-old rat lens. Histological sections were prepared from formalin-fixed paraffin embedded OXYR and OXYS rat eyes. Sections were probed with a monoclonal antibody against HNE indicating lipid peroxidation using an immunoperoxidase method. Lens epithelial cells (nuclei faintly visible at arrows) and subjacent lens fibers in control OXYR (A and C) rats contain low levels of HNE, whereas levels of HNE in OXYS rats (B and D) are greatly increased. Note that no osmotic swelling of cortical fibers is observed (A and B). Locator diagrams show the regions where the images were taken. Capsule is 'c'. No color or tone adjustments were made to the original digital images. 400 × .

plasma membranes (Fig. 8(B), arrows). Whereas the textures of the unaffected cells all appear similarly uniform in staining, the disrupted cells displayed a variety of appearances. At intermediate magnification it was clear that there were at least two distinct patterns (Fig. 8(C)), one showing large non-stained fusiform streaks of irregular width (Fig. 8(C), arrows) and another showing a tangled fibrillar arrangement with numerous linear, curved and branched fibrils having nearly constant diameters (Fig. 8(C), arrowheads). At high magnification the fibrils were comparable in diameter to single plasma membranes and quite distinct from typical fiber cell cytoplasm (Fig. 8(D)). The fibrillar structures appeared to be extended tubes or thin sheets cut edge-on with minimum stain excluding widths of about the same thickness as individual plasma membranes, 7–8 nm (Fig. 8(D), arrowheads). It should be noted that the stain excluding region of the membranes (Fig. 8(D), arrows) is 4–5 nm, significantly smaller than the thinnest observed unstained linear fibrillar structure. The cytoplasm where the fibrillar structures exist (Fig. 8(D), below membranes, red) does not exhibit the globular pattern typical of fiber cell cytoplasm (Fig. 8(D), above membranes, blue). Because the membranes at cellular interfaces appear intact, these images suggest that the disrupted cells and branched fibrils have a completely altered packing arrangement of the cytoplasmic proteins. In some cells (data not shown) the fibrillar pattern

blended into the typical globular smooth cytoplasm suggesting that there was an extensive reorganization or altered folding of polypeptide possibly induced by oxidative damage.

The rich variety of cellular damage observed within OXYS lenses raises the question of how relevant each type

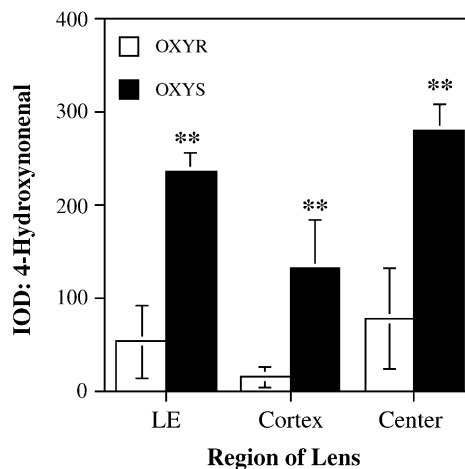


Fig. 4. Immunohistochemical measurement of 4-hydroxynonenal (HNE) in 1-month-old rat lenses. Histological sections of OXYR and OXYS rat eyes were prepared as described in Fig. 3. The density of product was quantitatively determined by comparison to optical standards. Five measurements in each location were made on six lenses. Significant differences at $p < 0.05$ are indicated by **.

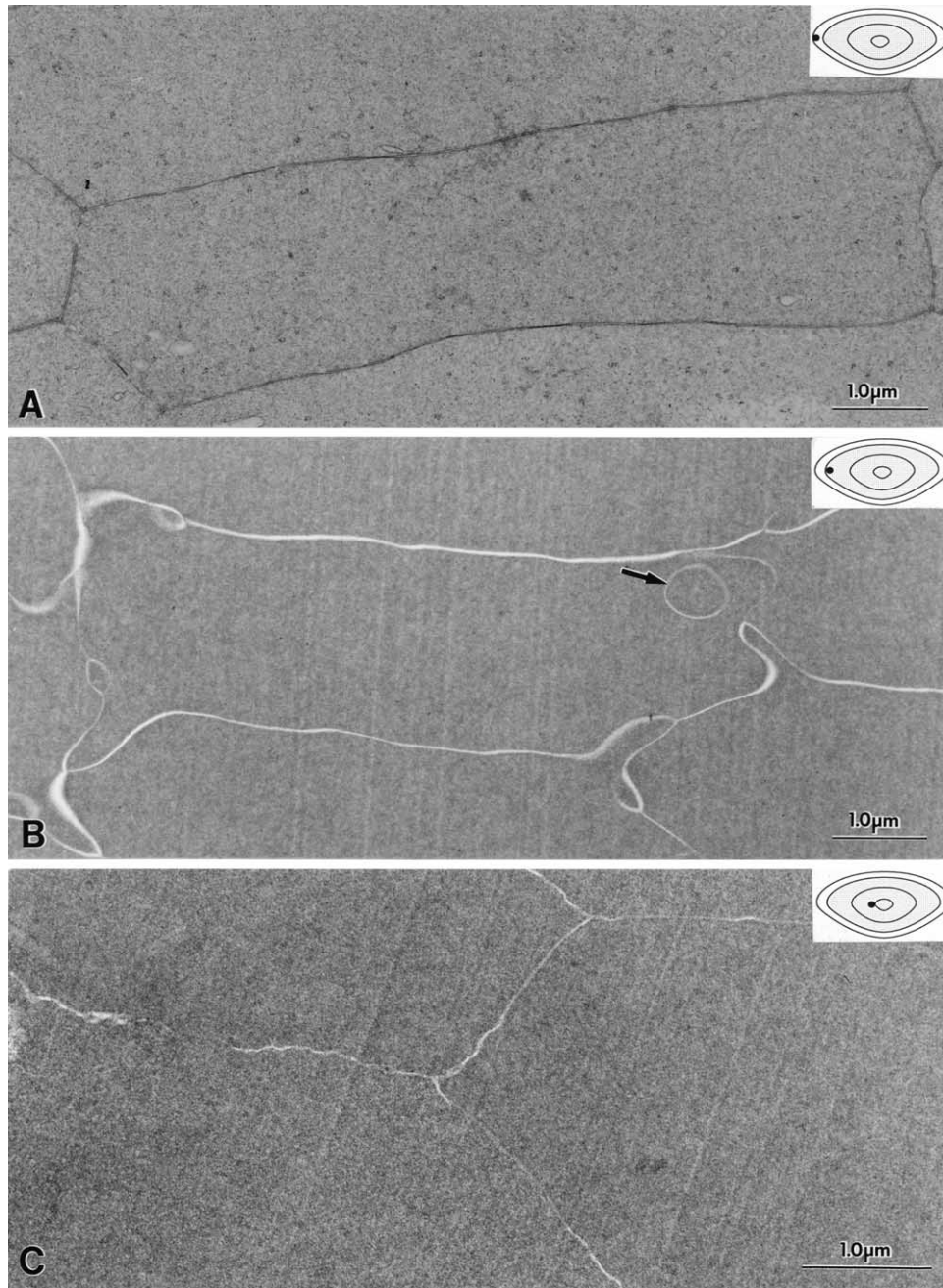


Fig. 5. Transmission electron micrographs of fiber cells from 6-month-old OXYR lenses. Cross-sections of fiber cells in the equatorial plane are shown from three developmental regions (locator diagrams). (A) Fiber cells of the outer cortex have large areas and a typical flattened hexagonal shape. The high staining contrast of the membranes reveals them as dark lines. (B) Deeper fiber cells of the adult nucleus are more irregular in shape and, because of the reduced contrast, the membranes appear as white lines. A circular profile (arrow) that can often appear within the cytoplasm is most likely a section through an interdigitation. (C) Fiber cells from the lens center usually have large cross-sectional areas, often are irregular in shape and have smooth homogeneous cytoplasm (Al-Ghoul and Costello, 1997).

of damage is to human cataract formation. Of particular importance is the textured cytoplasm of the fetal and embryonic nuclei (Fig. 6(D)) because the non-homogeneous distribution of stain could indicate the chemical modification and condensation of the crystallins, which is the hypothetical basis for nuclear cataract formation (Benedek, 1997). During the Vibratome sectioning of fresh adult OXYS lenses, this inner nuclear region was observed to be

cloudy or turbid compared to the clear OXYR lens nuclei (data not shown). This assessment could not be made on intact lenses because the complete opacity of the outer nuclear region obscured the view of the inner nucleus (Fig. 1(A) and (D)). In order to investigate the potential of the textured cytoplasm to explain nuclear light scattering, Fourier analysis techniques were used to examine equivalent regions of OXYR and OXYS nuclear cytoplasm (Fig. 9).

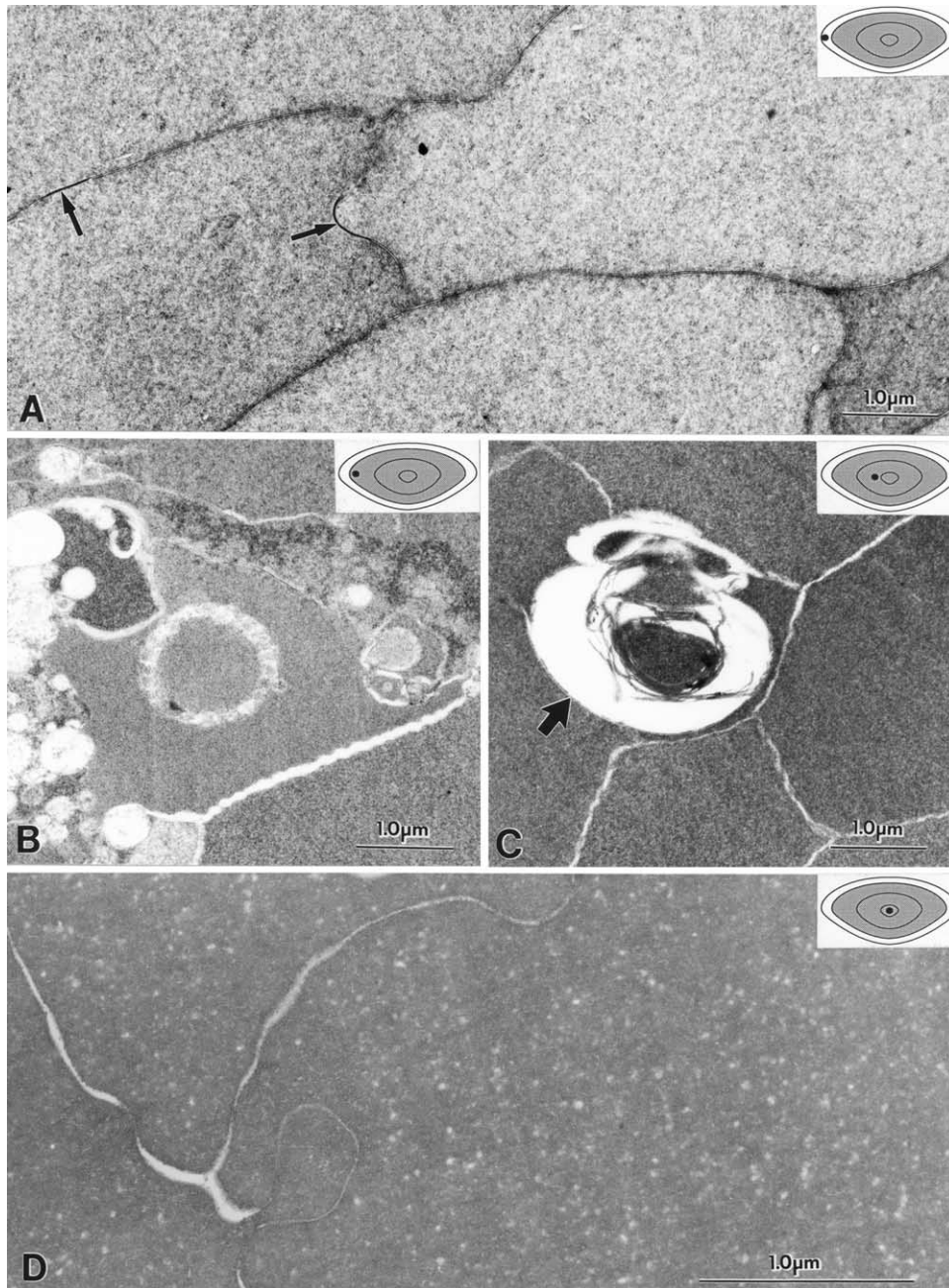


Fig. 6. Transmission electron micrographs of fiber cells from 6-month-old OXYS lenses. Cross-sections in the equatorial plane in four developmental regions (locator diagrams). (A). Fiber cells of the outer cortex are swollen and irregular. Two gap junctions are indicated (arrows). (B). Cell disruption is seen at the cortex/nucleus interface. (C). Massive disruption of one cell surrounded by apparently undamaged cells in the fetal nucleus. Multiple layers of thin membranes surround a dense central core in this 2- μm diameter object (arrow). (D). Fiber cells of the embryonic nucleus display a highly textured cytoplasm caused, in part, by numerous small white low density spots or voids.

Images at $21\,000\times$ and their Fourier transforms support the impression of irregular distribution of the cytoplasmic components in the OXYS (Fig. 9(C) and (D)) compared to the OXYR (Fig. 9(A) and (C)). The 3D representation and color coding of the amplitude of the Fourier components (Fig. 9(B) and (D)) emphasizes the shift of components from outer high frequency toward inner lower frequency (smaller diameter green and red zones in Fig. 9(D)) and the large increase in components at low frequency near

the center (yellow peak). These changes are quantitatively represented by plots of the radial average of intensity (Fig. 9(E)). The difference in the radial average plots produces a pronounced peak near $1/100\text{ nm}$ indicating a dramatic increase in the stain density fluctuations in the equivalent size range of $100\text{--}300\text{ nm}$ (Fig. 9(E), red line). This analysis is consistent with previous Fourier analyses comparing human and animal lens nuclear cytoplasm (Freel et al., 2002).

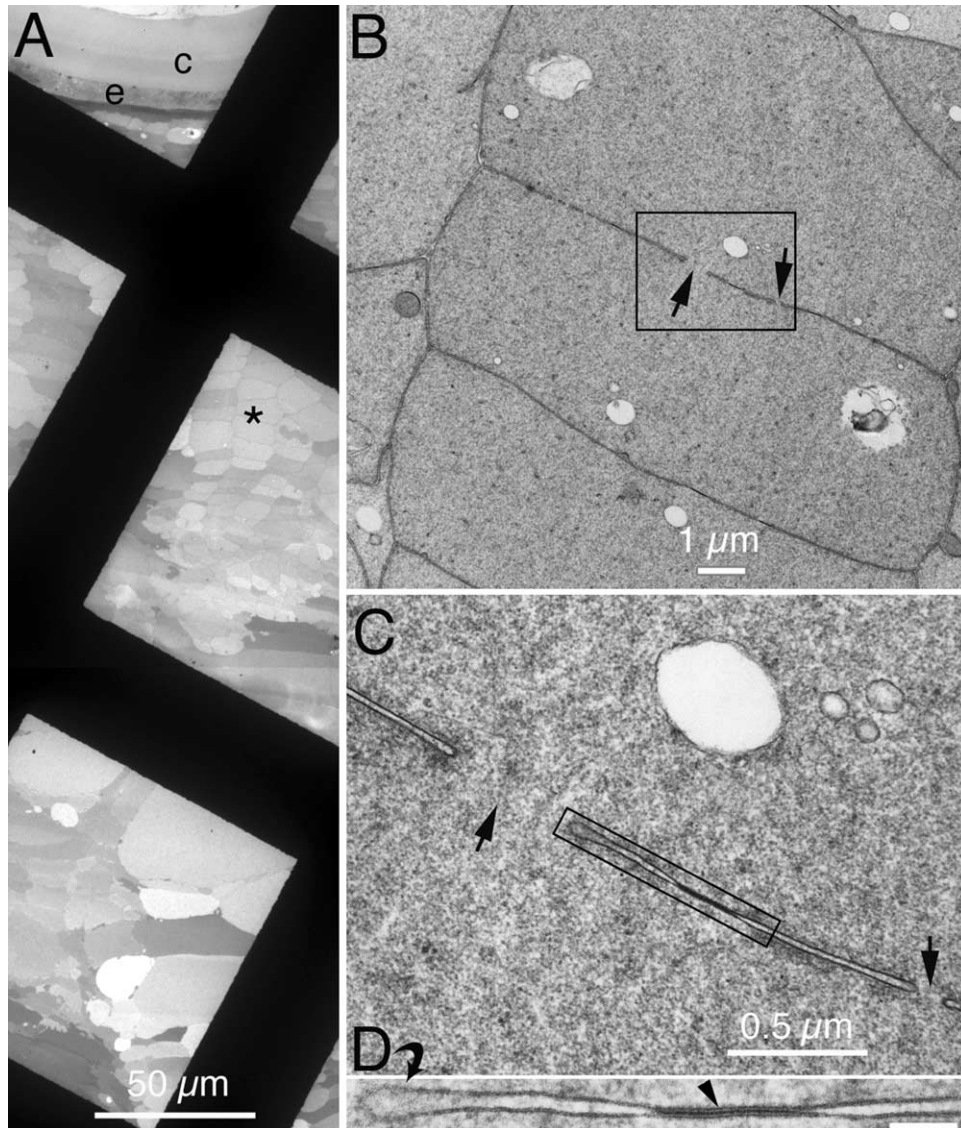


Fig. 7. Cortical region containing numerous sites of cell-to-cell fusion. (A). Overview of a thin section in the equatorial plane at the lens surface. Capsule 'c' and epithelium 'e' are indicated. The region of excess fusion sites is 50–100 μm from the surface (*) within the zone of organelle degeneration. A region of swollen cells occurs about 200 μm from the surface. The black stripes are opaque bars of the supporting 200-mesh grid. (B). Intermediate magnification reveals fusion sites between adjacent cells (arrows). Boxed area is enlarged. Other cells in this region have multiple fusion sites. (C). Each fusion site (arrows) is characteristically bordered by a loop of membrane, which in three dimensions would be an annulus. The rectangular region is enlarged. (D). At high magnification the membrane forming the loop is visible. Frequently, pentalamellar fiber cell junctions are present (arrowhead).

The Fourier analysis was also used to estimate opacity of the samples examined in thin section electron microscope images by making two assumptions. First, it was assumed that the heavy metals stain cytoplasmic proteins non-specifically and, second, it was assumed that the density of stain is related to the concentration of protein and thus to the local refractive index. It was then possible to assign a refractive index scale to the density of stain in images and derive an expression of the light scattered (representing opacity) as a function of the wavelength of light scattered (see Section 2). This process is essentially placing the Fourier amplitudes on a realistic scale from which refractive index fluctuations can be evaluated. Scattering curves thus calculated (Fig. 9(F), red and blue lines) show the similarity

of the OXYS and OXYR cytoplasm at low wavelengths and a distinct and pronounced difference in scattering of wavelengths in the visible region (Fig. 9(F), yellow band). The ratio of the scattering curves (Fig. 9(F), green line) further emphasizes the differences and supports the conclusion that the object with the density fluctuations seen in the original image (Fig. 9(C)) would be turbid or have high opacity, consistent with the opaque appearance of the fresh cataractous lens nucleus.

4. Discussion

The ultrastructural analysis of the adult OXYS rat cataractous lenses confirms the presence of varied and

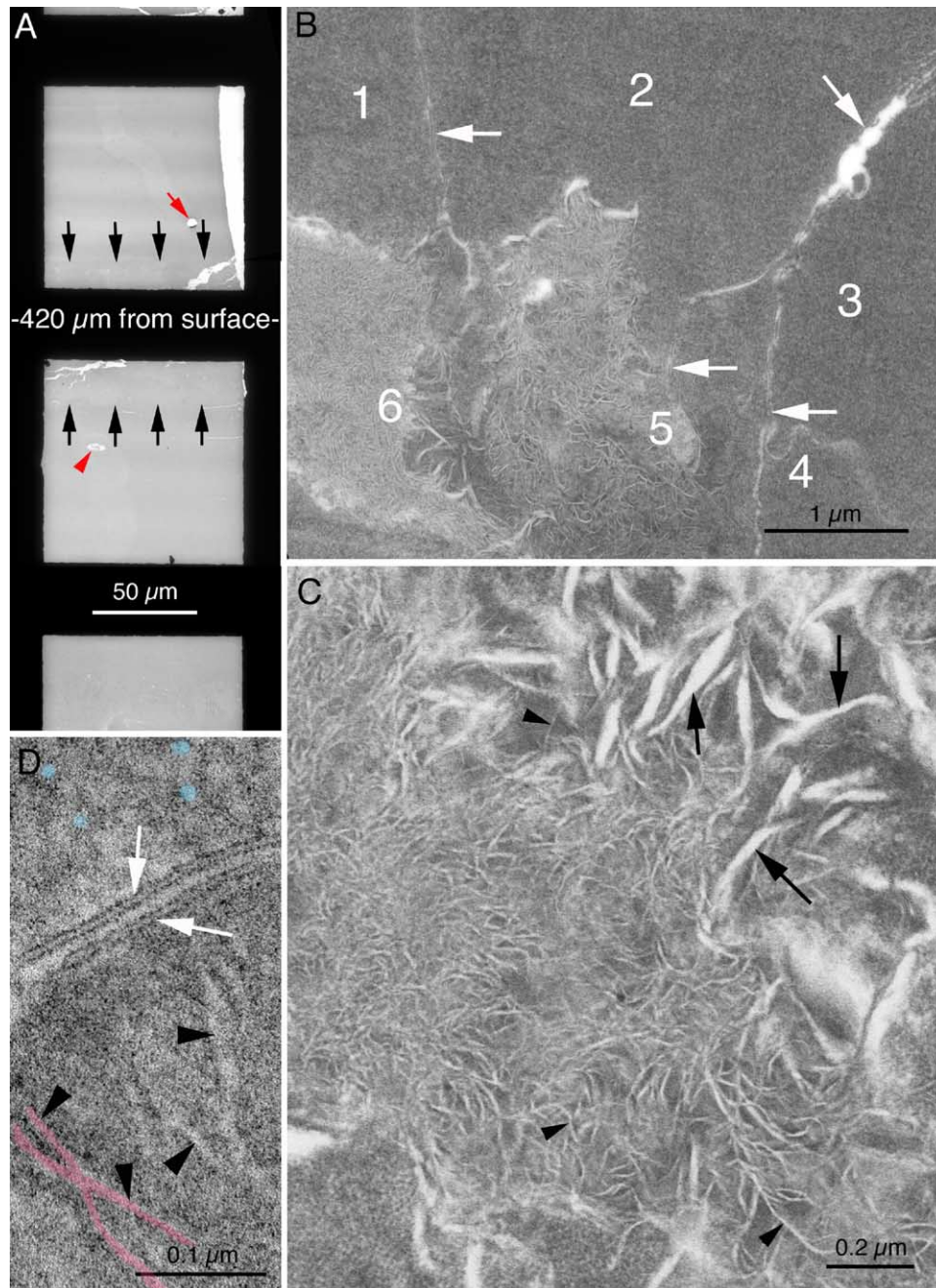


Fig. 8. A new form of fiber cell damage in OXYS adult nucleus. (A). Overview of a thin section in the region 420 μm from the lens surface in the equatorial plane. Unusual cellular damage is observed between the sets of arrows on both sides of the grid bar. Cells on either side of this region are relatively normal, although occasional globular bodies are visible (red arrowhead). A small tear (red arrow) and several cracks are typical features of the preparation method. (B). Low magnification views of cells 1–4 illustrate normal cytoplasmic morphology, whereas cells 5–6 show extensive fibril-like disruption of the cytoplasm. Typical membranes are visible between adjacent cells (arrows). (C). Enlarged view of a cell adjacent to the field in B showing two distinctive patterns, a network of thin, branching fibrils of fairly constant diameter (arrowheads) and large irregularly shaped fusiform stain excluding regions (arrows) most often seen on the outside of the fibrillar clusters. (D). High magnification view of two plasma membranes (arrows) and four thin fibrillar structures (arrowheads). Two crossing fibrils are colored red. Typical cytoplasm composed of globular subunits (examples in blue) is present in the upper left of the image. Note the dense staining surfaces of the membranes (producing the railroad track appearance) and the absence of such staining around the fibrils.

extensive cellular damage. Consistent with previous reports on human and rabbit lenses (Al-Ghoul and Costello, 1993; Costello et al., 1993; Al-Ghoul et al., 1996), the distinctive types of cellular disruption are characteristic of the developmental region in which they occur. Thus, cell

swelling and globular formation occur at the cortex/nucleus interface, multilamellar globular bodies occur mainly in the adult and fetal nuclei and redistribution of cytoplasmic protein (cytoplasmic texturing) occurs in the fetal and embryonic nuclei (Fig. 6). Other unusual types of damage

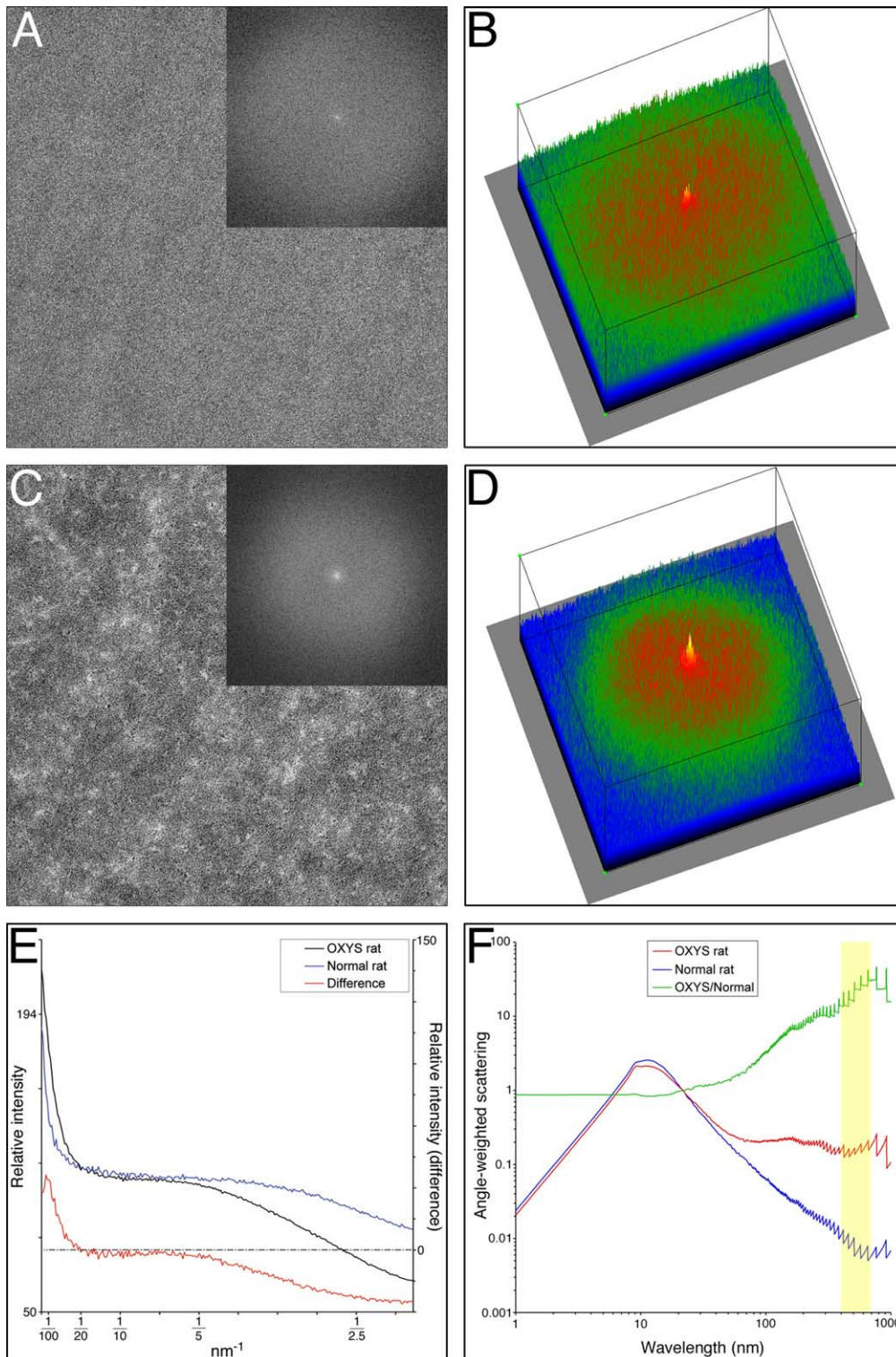


Fig. 9. Fourier analysis of nuclear cytoplasmic texture from control ($n = 2$) and OXYS ($n = 3$) rat lenses. High-magnification ($21\,000\times$) images of inner nuclear cytoplasm from control (A) and OXYS (C) rat lenses with inset two-dimensional Fourier spectra. Surface plots of the spectra better illustrate the increase in large cytoplasmic components as evident by the larger central peak in the OXYS specimens (D) compared to the controls (B). By averaging the radial magnitudes of many spectra (3–10 per specimen), an averaged plot for each sample group is produced comparing control OXYR and OXYS cytoplasmic texture (E). Subtracting the averaged normal OXYR curve from the OXYS produces a difference curve illustrating an increase in large cytoplasmic components of 50 nm and greater in the OXYS animals. Note that the averaged curves use the left intensity scale, while the difference curve uses the scale on the right. The amount of observed opacity with such changes in cytoplasmic organization can be predicted theoretically, and is graphically displayed in (F). This chart illustrates a disparity in angle-weighted scattering between control and OXYS nuclear cytoplasm, with the OXYS scattering nearly fifty times more visible light (400–700 nm) than the transparent control tissue.

were also observed. A narrow region in the outer cortex contained an unusually large number of fusion sites that indicated damage to the membranes or the loss of inhibition to fusion of adjacent fiber cell membranes (Fig. 7). Deeper in the adult nucleus was a region only 100 μm wide that contained unique fibrillar-like cytoplasm suggesting a massive alteration in the conformation and packing of crystallins (Fig. 8). It is attractive to hypothesize that all of these varied structural alterations are caused by oxidative damage from the innate high levels of ROS characteristic of the OXYS strain.

Support for the direct involvement of oxidative damage is provided by the histochemical evidence of increased oxidative breakdown products of DNA (Fig. 2(A)). Together with the images that show lens epithelial hyperplasia and PAS-positive excess basement membrane material (Fig. 2(C)–(E)), the data support the conclusion that the epithelial cells, and possibly the newly formed fibers, are adversely affected in OXYS lenses. Further direct evidence for oxidative damage is the increased level of HNE indicating extensive lipid peroxidation throughout the OXYS lens (Figs. 3 and 4). The damage to phospholipids may alter the membrane composition and stability, which could increase the number of fusion sites in the outer cortical zone (Fig. 7), well outside the organelle-free zone reported to have occasional cell fusion sites within chicken and mammalian lenses (Kuszak et al., 1985; Shestopalov and Bassnett, 2000, 2003). In addition, the reactive aldehyde HNE, and perhaps other products of LPO, may alter proteins and membrane structures (Ansari et al., 1996).

The source of excess ROS in OXYS lenses is not fully resolved. One of the key features of the OXYS rats is that the main defect involves a single gene that appears to enhance glucose uptake (Solovyova et al., 1987). The excess cellular glucose may cause diabetic-like conditions, even though the animals have normal blood glucose and are not diabetic. The excess cellular glucose may trigger the aldose reductase pathway that consumes the NADPH cofactor necessary for glutathione reductase to maintain GSH levels; lower amounts of GSH may lead to greater oxidative damage (Lee et al., 1995; Lee and Chung, 1999). The glucose itself may autoxidize to produce ROS (Thornalley et al., 1984; Wolff and Dean, 1987), as well as glycate crystallins, causing crystallin cross-linking and modified protein packing (Monnier, 1990). These changes caused by oxidative damage and excess glucose are probably sufficient to account for the non-homogeneous, highly textured cytoplasm of the inner nuclear regions. Textured cytoplasm was reported for a human nucleus from a late-onset diabetic patient (Al-Ghoul and Costello, 1996), and the canine model with spontaneous diabetes produced a similar highly textured cytoplasm (Taylor et al., 1997).

The treatment of animals with drugs or environmental challenges has generated many models of cataract formation with oxidative stress as a component. These include galactose induced osmotic cataracts in rodents

(Kuwabara et al., 1969; Ai et al., 2000), similar models of drug induced diabetes in several species (Costello et al., 1993; Swamy-Mruthinti et al., 1999), exposure to UV radiation (Michael et al., 2000; Giblin et al., 2002) or hyperbaric oxygen (Giblin et al., 1995; Padgaonkar et al., 1999) and administration of many compounds, such as naphthalene (Xu et al., 1992), and sodium selenite (Shearer et al., 1997). Each of these models has attempted to emphasize one or a few features of the cataractous process including the formation of nuclear cataracts. Especially valuable are the accompanying biochemical analyses that establish common features with other animal models and with human cataract formation. For example, exposure of guinea pigs to UV radiation (Giblin et al., 2002) and hyperbaric oxygen (Giblin et al., 1995; Freel et al., 2003) produce increased scattering almost entirely within the nucleus. These treatments also definitively increase thiol oxidation, as well as other oxidative damage to lens proteins and membranes (Borchman et al., 2000). However, these models display only mild nuclear scattering, similar to aging human lenses, rather than nuclear opacification typical of human age-related nuclear cataracts (Freel et al., 2002). Administration of some compounds, such as naphthalene, can generate mature cataracts containing damaging metabolic byproducts that may act through similar mechanism to oxidative damage (Xu et al., 1992). The administration of selenite seems to disrupt oxidative defense mechanisms, as well as elevate calcium and turn on degradative enzymes (Shearer et al., 1997). The mechanism of damage is being actively investigated and may be directly relevant to human cataract formation. However, because of the method of initiation and variable response to selenite in different species, it is likely that other animal models that generate ROS as the major source of oxidative damage may be more suitable for the study of human age-related cataracts.

Many features of OXYS rat suggest its suitability as model of age-related human cataracts. The most important factors are the early onset of lens scattering as detected by biomicroscopy and the involvement of the nucleus in cataract formation within months, which is promising for longitudinal studies and for sorting out the influence of aging and stress factors. Moreover, the globular bodies containing many stacked thin membranes are similar to the multilamellar bodies found in the nuclei of age-related nuclear cataracts (Gilliland et al., 2001). Changes in the cytoplasm of the inner nucleus are also important because the texturing and accompanying turbidity suggests a correlation between cytoplasmic protein rearrangements and increased scattering (Benedek, 1997). None of these features was observed in OXYR lenses.

Other properties of the adult OXYS cataractous lenses are not commonly observed in humans or other models. Specifically, the presence of cytoplasm composed of an apparently complex tangle of fibrils has not been reported previously (Fig. 8). Although a full understanding of the molecular arrangement of the fibrillar cytoplasm is not yet

available, it appears that membrane components are not likely to account for the extensive alterations in the cytoplasm (Fig. 8(D)). Several possible explanations for modifications of the cytoplasmic proteins can be offered. Evidence is mounting that amyloid-like deposits occur in human and animal cataractous lenses (Frederikse and Ren, 2002; Goldstein et al., 2003). The prevalence of beta secondary structure in the crystallins correlates with the fiber formation of amyloid proteins (Malinchik et al., 1998; Goldsbury et al., 2000; Green et al., 2003; Meehan et al., 2004). It is possible that oxidative damage to crystallins promotes the formation of fibrils; however, the ultrastructure of natural and artificial amyloid fibers is different from the OXYS fibrillar pattern of thin, curved and branching strands that have smooth borders (Fig. 8). Notably, the stain used for TEM would normally darken the protein fibers (Malinchik et al., 1998) whereas the OXYS fibrils exclude the stains indicating high hydrophobicity or tight packing that inhibits binding. Further analysis of the OXYS adult lenses is needed using specific stains for amyloid and markers for the key protein conformations to evaluate this intriguing possibility.

Another possibility is the crystallization of the cytoplasmic proteins or other non-protein components. Several localized scattering centers have been postulated to contain crystalline material, such as calcium oxalate (Harding et al., 1983; Vrensen et al., 1994; Mumford et al., 2000; Pande et al., 2001). The crystals may exclude heavy metal stains, although the morphology of the crystals described to date do not match the pattern of fibrils observed. The most promising correlation is with human lens retrodots that appear in the deep cortex and adult nucleus (Vrensen et al., 1994). These isolated oval scattering centers range in size from 25 to over 500 μm and possibly contain high calcium trapped by oxalate or phosphate. Of particular interest is the scanning electron microscopic view of the retrodots, which appear to be aggregates of thin sheets that are straight or slightly curved. Even though the objects reported are much larger than those observed by TEM (Fig. 8), it is reasonable to imagine that a thin section cut through the retrodots could produce thin stain-excluding bands that have the appearance of fibrils.

A third possibility is the reorganization of the crystallins, especially alpha crystallin (Horwitz, 2003). Structural studies demonstrate that alpha crystallin forms roughly 14–16 nm diameter spherical particles composed of about 32 monomers assembled with a hydrophobic core (Siezen et al., 1978; Haley et al., 1998) characteristic of small heat shock proteins (Kim et al., 1998; Haley et al., 2000; Van Montfort et al., 2001). It may be possible that oxidative damage to alpha crystallin is sufficient to produce a conformational change and subunit reorganization that opens the spherical assembly of monomers. This process may expose the hydrophobic interior and promote the aggregation of crystallins into tubes and thin sheets that have stain excluding hydrophobic cores. This interpretation

would be consistent with the diameter of the smaller strands and the staining pattern in the thin sections (Fig. 8). Clearly, more work needs to be done to characterize these unusual patterns.

The most widely accepted hypothesis for human nuclear cataract formation is the aggregation and precipitation of modified lens crystallins, mainly by oxidative damage, resulting in domains of high refractive index (Benedek, 1997). The protein condensation hypothesis predicts that the cytoplasm of the nuclear fiber cells is a mixture of high refractive index regions of condensed protein surrounded by low refractive index regions, producing a textured cytoplasm having fluctuations in refractive index and increased light scattering (Bettelheim, 1985). We have used Fourier analysis to quantify the cytoplasmic texture of the OXYS and OXYR lenses (Fig. 9). The observed increased amplitude of the Fourier components at low frequency (closer to the center) for the OXYS compared to the OXYR nuclear fiber cytoplasm suggests that the OXYS is more textured and has larger refractive index fluctuations. The difference in the radial average plots shows a pronounced peak between 1/200 and 1/100 nm (Fig. 9(E)), which is the size of fluctuations expected to produce significant scattering (Clark, 1994). The smooth cytoplasmic texture of the OXYR cytoplasm is consistent with a transparent lens and the highly textured cytoplasm of the OXYS is consistent with the observed high scattering from the nucleus. The Fourier analysis of the OXYS is similar to that of the diabetic canine (Taylor et al., 1997) and reveals greater refractive index fluctuations than in hyperbaric oxygen treated guinea pigs and in human nuclear cataract (Freel et al., 2002, 2003).

An extension of the Fourier analysis of texture is introduced here to relate cytoplasmic textural variations to in vivo opacity, also expressed as turbidity or angle-weighted scattering (Fig. 9(F)). For these calculations to be successful, it was necessary to make some reasonable assumptions about the relationship of the optical density of heavy metal stain in TEM images to the local refractive index. Because refractive index is related to protein concentration and heavy metals typically stain protein in proportion to its concentration, the darkest and lightest staining regions were assigned refractive index values, thus giving a range of indices corresponding to the grayscale range of the images. The Fourier analysis faithfully captures the local density fluctuations in the images and the theoretical analysis (see Section 2) relates these variations to the expected scattering. As a function of wavelength of light, the angle-weighted scattering is calculated for a real object that has an internal organization as seen in the high-resolution TEM images. Therefore, in the low wavelength region, which is not relevant to human vision, the scattering is similar; however, for wavelengths in the visible region, the scattering is much greater for the OXYS cytoplasm. The ratio emphasizes the greater scattering from the OXYS cytoplasm consistent with the observed opacity of the nucleus of the real lens. For the first time it is now possible

to obtain predicted scattering in real space (not Fourier space) of lenses based on the internal ultrastructure of the normal transparent and cataractous lenses.

Acknowledgements

The authors are grateful to W. Lane and H. Mekeel for expert technical assistance. This work was supported in part by funds from NIH Grants EY08148 and EY05722.

References

- Ai, Y., Zheng, Z., O'Brien-Jenkins, A., Bernard, D.J., Wynshaw-Boris, T., Ning, C., Reynolds, R., Segal, S., Huang, K., Stambolian, D., 2000. A mouse model of galactose-induced cataracts. *Hum. Mol. Genet.* 9, 1821–1827.
- Al-Abdulla, N.A., Martin, L.J., 1998. Apoptosis of retrogradely degenerating neurons occurs in association with the accumulation of perikaryal mitochondria and oxidative damage to the nucleus. *Am. J. Pathol.* 153, 447–456.
- Albright, C.D., Friederich, C.B., Brown, E.C., Mar, M.H., Zeisel, S.H., 1999. Maternal dietary choline availability alters mitosis, apoptosis and the localization of TOAD-64 protein in the developing fetal rat septum. *Brain Res. Dev. Brain Res.* 113, 13–20.
- Albright, C.D., Zeisel, S.H., Salganik, R.I., 1998. Choline deficiency induces apoptosis and decreases the number of eosinophilic preneoplastic foci in the liver of OXYS rats. *Pathobiology* 66, 71–76.
- Al-Ghoul, K.J., Costello, M.J., 1993. Morphological changes in human nuclear cataracts of late-onset diabetics. *Exp. Eye Res.* 57, 469–486.
- Al-Ghoul, K.J., Costello, M.J., 1996. Fiber cell morphology and cytoplasmic texture in cataractous and normal human lens nuclei. *Curr. Eye Res.* 15, 533–542.
- Al-Ghoul, K.J., Costello, M.J., 1997. Light microscopic variation of fiber cell size, shape and ordering in the equatorial plane of bovine and human lenses. *Mol. Vis.* 3, 2.
- Al-Ghoul, K.J., Lane, C.W., Taylor, V.L., Fowler, W.C., Costello, M.J., 1996. Distribution and type of morphological damage in human nuclear age-related cataracts. *Exp. Eye Res.* 62, 237–251.
- Ames, B.N., Shigenaga, M.K., Hagen, T.M., 1993. Oxidants, antioxidants, and the degenerative diseases of aging. *Proc. Natl Acad. Sci. USA* 90, 7915–7922.
- Ansari, N.H., Wang, L., Srivastava, S.K., 1996. Role of lipid aldehydes in cataractogenesis: 4-hydroxynonenal-induced cataract. *Biochem. Mol. Med.* 58, 25–30.
- Awasthi, S., Srivastava, S.K., Piper, J.T., Singhal, S.S., Chaubey, M., Awasthi, Y.C., 1996. Curcumin protects against 4-hydroxy-2-nonenal-induced cataract formation in rat lenses. *Am. J. Clin. Nutr.* 64, 761–766.
- Babizhayev, M.A., Arkhipenko, I.V., Kagan, V.E., 1987. Antioxidative enzyme activity and metabolism of peroxide compounds in the crystalline lens during cataractogenesis. *Bull. Eksp. Biol. Med.* 103, 143–146.
- Babizhayev, M.A., Deyev, A.I., Linberg, L.F., 1988. Lipid peroxidation as a possible cause of cataract. *Mech. Aging Dev.* 44, 69–89.
- Baldwin, S.A., Broderick, R., Osbourne, D., Waeg, G., Blades, D.A., Scheff, S.W., 1998. The presence of 4-hydroxynonenal/protein complex as an indicator of oxidative stress after experimental spinal cord contusion in a rat model. *J. Neurosurg.* 88, 874–883.
- Benedek, G.B., 1997. Cataract as a protein condensation disease. The Proctor lecture. *Invest. Ophthalmol. Vis. Sci.* 38, 1911–1921.
- Bettelheim, F.A., 1985. Physical basis of lens transparency. In: Maisel, H., (Ed.), *The ocular lens*. Marcel Dekker, New York, pp. 265–300.
- Bhuyan, K.C., Bhuyan, D.K., Podos, S.M., 1986. Lipid peroxidation in cataract of the human. *Life Sci.* 38, 1463–1471.
- Bohren, C.F., 1987. Multiple scattering of light and some of its observable consequences. *Am. J. Phys.* 55, 524–533.
- Borchman, D., Giblin, F.J., Leverenz, V.R., Reddy, V.N., Lin, L.R., Yappert, M.C., Tang, D., Li, L., 2000. Impact of aging and hyperbaric oxygen in vivo on guinea pig lens lipids and nuclear light scatter. *Invest. Ophthalmol. Vis. Sci.* 41, 3061–3073.
- Charney, E., Brackett, F.S., 1961. The spectral dependence of scattering from a spherical alga cell and its implication for the state of organization of the light accepting pigments. *Arch. Biochem. Biophys.* 92, 1–12.
- Choudhary, S., Zhang, W., Zhou, F., Campbell, G.A., Chan, L.L., Thompson, E.B., Ansari, N.H., 2002. Cellular lipid peroxidation end-products induce apoptosis in human lens epithelial cells. *Free Radic. Biol. Med.* 32, 360–369.
- Clark, J.I. 1994. Development and maintenance of lens transparency. In: Albert, D.M., Jakobiec, F.A. (Eds.), *Principles and practice of ophthalmology*. W.B. Saunders, Philadelphia, pp. 143–123.
- Clark, J.I., 2001. Fourier and power law analysis of structural complexity in cornea and lens. *Micron* 32, 239–249.
- Costello, M.J., Lane, C.W., Hatchell, D.L., Saloupis, P., Cobo, L.M., 1993. Ultrastructure of fiber cells and multilamellar inclusions in experimental diabetes. *Invest. Ophthalmol. Vis. Sci.* 34, 2174–2185.
- Costello, M.J., Marsili, S., Lane, C.W., Salganik, R.I., Albright, C.D., Peiffer, R.L., 2000. Cataract formation in a strain of rats selected for high oxidative stress. *Microsc. Microanal.* 6, 590–591.
- Font, R.L., Brownstein, S., 1974. A light and electron microscopic study of anterior subcapsular cataracts. *Am. J. Ophthalmol.* 78, 972–984.
- Frederikse, P.H., Ren, X.-O., 2002. Lens defects and age-related fiber cell degeneration in a mouse model of increased AbetaPP gene dosage in Down Syndrome. *Am. J. Pathol.* 161, 1985–1990.
- Freegard, T.J., 1997. The physical basis of transparency in the normal cornea. *Eye* 11, 465–471.
- Freel, C.D., Gilliland, K.O., Lane, C.W., Giblin, F.J., Costello, M.J., 2002. Fourier analysis of cytoplasmic texture in nuclear fiber cells from transparent and cataractous human and animal lenses. *Exp. Eye Res.* 74, 689–702.
- Freel, C.D., Gilliland, K.O., Mekeel, H.E., Giblin, F.J., Costello, M.J., 2003. Ultrastructural characterization and Fourier analysis of fiber cell cytoplasm in the hyperbaric oxygen treated guinea pig lens opacification model. *Exp. Eye Res.* 76, 405–415.
- Giblin, F.J., Padgaonkar, V.A., Leverenz, V.R., Lin, L.R., Lou, M.F., Unakar, N.J., Dang, L., Dickerson, J.E. Jr., Reddy, V.N., 1995. Nuclear light scattering, disulfide formation and membrane damage in lenses of older guinea pigs treated with hyperbaric oxygen. *Exp. Eye Res.* 60, 219–235.
- Giblin, F.J., Leverenz, V.R., Padgaonkar, V.A., Unakar, N.J., Dang, L., Lin, L.R., Lou, M.F., Reddy, V.N., Borchman, D., Dillon, J.P., 2002. UVA light in vivo reaches the nucleus of the guinea pig lens and produces deleterious, oxidative effects. *Exp. Eye Res.* 75, 445–458.
- Gilliland, K.O., Freel, C.D., Lane, C.W., Fowler, W.C., Costello, M.J., 2001. Multilamellar bodies as potential scattering particles in human age-related nuclear cataracts. *Mol. Vis.* 7, 120–130.
- Gisselberg, M., Clark, J.I., Vaezy, S., Osgood, T.B., 1991. A quantitative evaluation of Fourier components in transparent and opaque calf cornea. *Am. J. Anat.* 191, 408–418.
- Glauert, A.M., 1965. Section staining, cytology, autoradiography, and immunochemistry for biological specimens. In: Kay, D.H., (Ed.), *Techniques for Electron Microscopy*. Blackwell, Oxford, pp. 254–310.
- Goldsbury, C.S., Wirtz, S., Muller, S.A., Sunderji, S., Wicki, P., Aebi, U., Frey, P., 2000. Studies on the in vitro assembly of A β 1-40: implications for the search for A β fibril formation inhibitors. *J. Struct. Biol.* 130, 217–231.
- Goldstein, L.E., Muffat, J.A., Cherny, R.A., Moir, R.D., Ericsson, M.H., Huang, X., Mavros, C., Coccia, J.A., Faget, K.Y., Masters, C.L.,

- Chylack, L.T., Bush, A.I., 2003. Cytosolic beta-amyloid deposition and supranuclear cataracts in lenses from people with Alzheimer's disease. *Lancet* 61, 1258–1265.
- Green, J., Goldsbury, C., Mini, T., Sunderji, S., Frey, P., Kistler, J., Cooper, G., Aebi, U., 2003. Full-length rat amylin forms fibrils following substitution of single residues from human amylin. *J. Mol. Biol.* 326, 1147–1156.
- Haley, D.A., Bova, M.P., Huang, Q.-L., Mchaourab, H.S., Stewart, P.L., 2000. Small heat-shock protein structures reveal a continuum from symmetric to variable assemblies. *J. Mol. Biol.* 298, 261–272.
- Haley, D.A., Horwitz, J., Stewart, P.L., 1998. The small heat-shock protein, α B-crystallin, has a variable quaternary structure. *J. Mol. Biol.* 277, 27–35.
- Harding, J.J., 2001. Can drugs or micronutrients prevent cataract? *Drugs Aging* 18, 473–486.
- Harding, C.V., Chylack, L.T. Jr., Susan, S.R., Lo, W.-K., Bobrowski, S.F., 1983. Calcium-containing opacities in the human lens. *Invest. Ophthalmol. Vis. Sci.* 24, 1194–1202.
- Hayat, M.A., 1971. *Principles and Techniques of Electron Microscopy: Biological Applications*. vol. 1. Van Nostrand Reinhold, New York.
- Hecht, E., 1998. *Optics*. Addison Wesley/Longman, New York, NY.
- Horwitz, J., 2003. Alpha-crystallin. *Exp. Eye Res.* 76, 145–153.
- Hosokawa, M., Ashida, Y., Tsuboyama, T., Chen, W.H., Takeda, T., 1984. Cataract and other ophthalmic lesions in senescence accelerated mouse (SAM). Morphology and incidence of senescence associated ophthalmic changes in mice. *Exp. Eye Res.* 38, 105–114.
- Inlay, J.A., Linn, S., 1988. DNA damage and oxygen radical toxicity. *Science* 240, 1302–1309.
- Ishchenko, A., Sinitsyna, O., Krysanova, Z., Vasyunina, E., Saparbaev, M., Sidorkina, O., Nevinsky, G., 2003. Age-dependent increase of 8-oxoguanine-, hypoxanthine-, and uracil- DNA glycosylase activities in liver extracts from OXYS rats with inherited overgeneration of free radicals and Wistar rats. *Med. Sci. Monit.* 9, 16–24.
- Johnsen, S., 2001. Hidden in plain sight: the ecology and physiology of organismal transparency. *Biol. Bull.* 201, 301–318.
- Kador, P.F., Fukui, H.N., Fukushi, S., Jernigan, H.M. Jr., Kinoshita, J.H., 1980. Philly mouse: a new model of hereditary cataract. *Exp. Eye Res.* 30, 59–68.
- Kim, K.K., Kim, R., Kim, S.-H., 1998. Crystal structure of a small heat-shock protein. *Nature* 394, 595–599.
- Kolosova, N.G., Aidagulova, S.V., Nepomnyashchikh, G.I., Shabalina, I.G., Shalbueva, N.I., 2001. Dynamics of structural and functional changes in hepatocyte mitochondria of senescence-accelerated OXYS rats. *Bull. Exp. Biol. Med.* 132, 814–819.
- Kuck, J.F., 1990. Late onset hereditary cataract of the Emory mouse. A model for human senile cataract. *Exp. Eye Res.* 50, 659–664.
- Kuszak, J.R., Macsai, M.S., Bloom, K.J., Rae, J.L., Weinstein, R.S., 1985. Cell-to-cell fusion of lens fiber cells in situ: correlative light, scanning electron microscopic and freeze-fracture studies. *J. Ulstruct. Res.* 93, 144–160.
- Kuwabara, T., Kinoshita, J.H., Cogan, D.G., 1969. Electron microscopic study of galactose-induced cataract. *Invest. Ophthalmol.* 8, 133–149.
- Lee, A.Y., Chung, S.S., 1999. Contributions of polyol pathway to oxidative stress in diabetic cataract. *FASEB J.* 13, 23–30.
- Lee, A.Y., Chung, S.K., Chung, S.S., 1995. Demonstration that polyol accumulation is responsible for diabetic cataract by the use of transgenic mice expressing the aldose reductase gene in the lens. *Proc. Natl Acad. Sci. USA* 92, 2780–2784.
- Li, W.C., Kuszak, J.R., Wang, G.M., Wu, Z.Q., Spector, A., 1995. Calcymycin-induced lens epithelial cell apoptosis contributes to cataract formation. *Exp. Eye Res.* 61, 91–98.
- Lipson, H., 1972. *Optical Transforms*. Academic Press, New York.
- Malinchik, S.B., Inouye, H., Szumowski, K.E., Kirschner, D.A., 1998. Structural analysis of Alzheimer's beta(1-40) amyloid: protofilament assembly of tubular fibrils. *Biophys. J.* 74, 537–545.
- Marsili, S., Salganik, R.I., Albright, C.D., Peiffer, R.L., Lane, C.W., Costello, M.J., 2000. Cataract formation in a high oxidative stress rat model. *Invest. Ophthalmol. Vis. Sci.* 41, S211.
- Meehan, S., Berry, Y., Luisi, B., Dobson, C.M., Carver, J.A., MacPhee, C.E., 2004. Amyloid fibril formation by lens crystalline proteins and its implication for cataract formation. *J. Biol. Chem.* 279, 3413–3419.
- Men'shchikova, E.B., Shabalina, I.G., Zenkov, N.K., Kolosova, N.G., 2002. Generation of reactive oxygen species by mitochondria in senescence-accelerated OXYS rats. *Bull. Exp. Biol. Med.* 133, 175–177.
- Michael, R., Vrensen, G.F., van Marle, J., Lofgren, S., Soderberg, P.G., 2000. Repair in the rat lens after threshold ultraviolet radiation injury. *Invest. Ophthalmol. Vis. Sci.* 41, 204–212.
- Michielsen, S., 1999. Specific refractive index increments of polymers in dilute solution. In: Brandup, J., Immergut, E.H., Grulke, E.A. (Eds.), *Polymer Handbook*. Fourth Ed., Wiley, New York, pp. 547–628.
- Minassian, D.C., Mehra, V., 1990. 3.8 million blinded by cataract each year: projections from the first epidemiological study of incidence of cataract blindness in India. *Br. J. Ophthalmol.* 74, 341–343.
- Monnier, V., 1990. Non-enzymatic glycosylation, the Maillard reaction and the aging process. *J. Geront.* 45, B105–B111.
- Mumford, A.D., Cree, I.A., Arnold, J.D., Hagan, M.C., Rixon, K.C., Harding, J.J., 2000. The lens in hereditary hyperferritinaemia cataract syndrome contains crystalline deposits of L-ferritin. *Br. J. Ophthalmol.* 84, 697–700.
- Nirmalan, P.K., Krishnadas, R., Tamakrishnan, R., Thulasiraj, R., Katz, J., Tielsch, J.M., Robin, A.I., 2003. Lens opacities in a rural population of southern India: the Aravind Comprehensive Eye Study. *Invest. Ophthalmol. Vis. Sci.* 44, 4639–4643.
- Okano, T., Uga, S., Ishikawa, S., Shumiya, S., 1993. Histopathological study of hereditary cataractous lenses in SCR strain rat. *Exp. Eye Res.* 57, 567–576.
- Padgaonkar, V.A., Lin, L.R., Leverenz, V.R., Rinke, A., Reddy, V.N., Giblin, F.J., 1999. Hyperbaric oxygen in vivo accelerates the loss of cytoskeletal proteins and MIP26 in guinea pig lens nucleus. *Exp. Eye Res.* 68, 493–504.
- Pande, A., Pande, J., Asherie, N., Lomakin, A., Ogun, O., King, J., Benedek, G.B., 2001. Crystal cataracts: human genetic cataract caused by protein crystallization. *Proc. Natl Acad. Sci.* 98, 6116–6120.
- Pokharel, G.P., Regmi, G., Shrestha, S.K., Negrel, A.D., Ellwein, L.B., 1998. Prevalence of blindness and cataract surgery in Nepal. *Br. J. Ophthalmol.* 82, 600–605.
- Prum, R.O., Torres, R., Williamson, S., Dyck, J., 1998. Coherent light scattering by blue feather barbs. *Nature* 396, 28–29.
- Prum, R.O., Torres, R., Williamson, S., Dyck, J., 1999a. Two-dimensional Fourier analysis of the spongy medullary keratin of structurally coloured feather barbs. *Proc. R. Soc. Lond. Ser. B. Biol. Sci.* 266, 13–22.
- Prum, R.O., Torres, R., Kovach, C., Williamson, S., Goodman, S.M., 1999b. Coherent light scattering by nanostructured collagen arrays in the caruncles of the Malagasy asities (Eurylaimidae: Aves). *J. Exp. Biol.* 202, 3507–3522.
- Salganik, R.I., 1979. Some patterns of protein synthesis in animal cells. In: Bush, H., (Ed.), *The Cell Nucleus*. Academic Press, New York, pp. 327–357.
- Salganik, R.I., 2001. The benefits and hazards of antioxidants: controlling apoptosis and other protective mechanisms in cancer patients and the human population. *J. Am. Col. Nutr.* 20, 464S–472S.
- Salganik, R.I., Solovyova, N.A., 1972. Induction of galactose-1-phosphate uridylyltransferase in rat liver under the effect of galactose and experimental galactosemia. *Vopr. Med. Khimii* 18, 72–77.
- Salganik, R.I., Solovyova, N.A., Grishaeva, O.N., Dikalov, S.I., Kandaurov, V.V., Semenova, L.A., 1994a. Inherited increase of free radical production in rat: development of pathological conditions. *Free Radic. Biol. Med.* 16, 13–14.
- Salganik, R.I., Solovyova, N.A., Grishaeva, O.N., Dikalov, S.I., Semenova, L.A., Popovskiy, A.V., 1994b. Inherited hyperproduction of free

- radicals. The pathology of aging. *Dokl. Russ. Akad. Nauk (Proc. Russ. Acad. Sci.)* 336, 255–258.
- Salganik, R.I., Solovyova, N.A., Dikalov, S.I., Grishaeva, O.N., Semenova, L.A., Popovsky, A.V., 1994c. Inherited enhancement of hydroxyl radical generation and lipid peroxidation in the S strain rats results in DNA rearrangements, degenerative diseases, and premature aging. *Biochem. Biophys. Res. Commun.* 199, 726–733.
- Salganik, R.I., Shabalina, I.G., Solovyova, N.A., Kolosova, N.G., Solovyov, V.N., Kolpakov, A.R., 1994d. Impairment of respiratory functions in mitochondria of rats with an inherited hyperproduction of free radicals. *Biochem. Biophys. Res. Commun.* 205, 180–185.
- Shearer, T.R., Ma, H., Fukiage, C., Azuma, M., 1997. Selenite nuclear cataract: review of the model. *Mol. Vis.* 3, 8.
- Shestopalov, V.I., Bassnett, S., 2000. Expression of autofluorescent proteins reveals a novel protein permeable pathway between cells in the lens core. *J. Cell Sci.* 113, 1913–1921.
- Shestopalov, V.I., Bassnett, S., 2003. Development of a macromolecular diffusion pathway in the lens. *J. Cell Sci.* 116, 4191–4199.
- Siezen, R.J., Bindels, J.G., Hoenders, H.J., 1978. The quaternary structure of bovine α -crystallin. *Eur. J. Biochem.* 91, 387–396.
- Solovyova, N.A., Ginzburg, E.Kh., Kazarinova, F.S., Kandaurov, V.V., Salganik, R.I., 1987. Elevated galactose transport into cells as the cause of development of hereditary galactosemia in rats. *Vopr. Med. Khim.* 33, 41–47.
- Solovyova, N.A., Morozkova, T.S., Salganik, R.I., 1975. Development of rat substrain with features of the hereditary galactosemia and studies of their biochemical features. *Genetika [Russ.]* 11, 63–70.
- Solovyova, N.A., Salganik, R.I., 1982. Studies of biochemical mechanisms of the development of hereditary galactosemia in W/SSM strain rats. *Genetika [Russ.]* 18, 420–427.
- Spector, A., 1984. The search for a solution to senile cataracts. *Invest. Ophthalmol. Vis. Sci.* 25, 130–146.
- Spector, A., 1995. Oxidative stress-induced cataract: mechanism of action. *FASEB J.* 9, 1173–1182.
- Struthers, L., Patel, R., Clark, J., Thomas, S., 1998. Direct detection of 8-oxodeoxyguanosine and 8-oxoguanine by avidin and its analogues. *Anal. Biochem.* 255, 20–31.
- Swamy-Mruthinti, S., Shaw, S.M., Zhao, H.-R., Green, K., Abraham, E.C., 1999. Evidence of a glycemic threshold for the development of cataracts in diabetic rats. *Curr. Eye Res.* 18, 423–429.
- Taylor, V.L., Al-Ghoul, K.J., Lane, C.W., Davis, V.A., Kuszak, J.R., Costello, M.J., 1996. Morphology of the normal human lens. *Invest. Ophthalmol. Vis. Sci.* 37, 1396–1410.
- Taylor, V.L., Costello, M.J., 1999. Fourier analysis of textural variations in human normal and cataractous lens nuclear fiber cell cytoplasm. *Exp. Eye Res.* 69, 163–174.
- Taylor, A., Nowell, T., 1997. Oxidative stress and antioxidant function in relation to risk for cataract. *Adv. Pharmacol.* 38, 515–536.
- Taylor, V.L., Peiffer, R.L., Costello, M.J., 1997. Ultrastructural analysis of normal and diabetic cataractous canine lenses. *Vet. Comp. Ophthalmol.* 7, 117–125.
- Thornalley, P., Wolff, S., Crabbe, J., Stern, A., 1984. The autoxidation of glyceraldehyde and other simple monosaccharides under physiological conditions catalysed by buffer ions. *Biochim. Biophys. Acta* 797, 276–287.
- Thylefors, B., 1995. Global data on blindness. *Bull. World Health Organ.* 73, 115–121.
- Thylefors, B., 1999. Avoidable blindness. *Bull. World Health Organ.* 77, 453.
- Tripathi, B.J., Tripathi, R.C., Borisuth, N.S., Dhaliwal, R., Dhaliwal, D., 1991. Rodent models of congenital and hereditary cataract in man. *Lens Eye Toxic. Res.* 8, 373–413.
- Truscott, R.J., 2000. Age-related nuclear cataract: a lens transport problem. *Ophthalmic Res.* 32, 185–194.
- Vaezy, S., Clark, J.I., 1994. Quantitative analysis of the microstructure of the human cornea and sclera using 2-D Fourier methods. *J. Microsc.* 175, 93–99.
- Vaezy, S.H., Clark, J.I., 1995. Characterization of the cellular microstructure of ocular lens using 2D power law analysis. *Ann. Biomed. Eng.* 23, 482–490.
- Vaezy, S., Clark, J.I., Clark, J.M., 1995. Quantitative analysis of the lens cell microstructure in selenite cataract using a two-dimensional Fourier analysis. *Exp. Eye Res.* 60, 245–255.
- Van Montfort, R.L., Basha, E., Friedrich, K.L., Slingsby, C., Vierling, E., 2001. Crystal structure and assembly of a eukaryotic small heat shock protein. *Nat. Struct. Biol.* 8, 1025–1030.
- Vrensen, G.F.J.M., Willekens, B., DeJong, P.T., Shun-Shin, G.A., Brown, N.P., Bron, A.J., 1994. Heterogeneity in ultrastructure and elemental composition of perinuclear lens retrodots. *Invest. Ophthalmol. Vis. Sci.* 35, 199–206.
- Whitfield, R., Schwab, L., Ross-Degnan, D., Steinkuller, P., Swartwood, J., 1990. Blindness and eye disease in Kenya: ocular status survey results from the Kenya Rural Blindness Prevention Project. *Br. J. Ophthalmol.* 74, 333–340.
- Wolff, S.P., 1994. Cataract and UV radiation. *Doc. Ophthalmol.* 88, 201–204.
- Wolff, S.P., Dean, R.T., 1987. Glucose autoxidation and protein modification. The potential role of autoxidative glycosylation in diabetes. *Biochem. J.* 245, 243–250.
- Xu, G.T., Zigler, J.S., Lou, M.F., 1992. Establishment of a naphthalene cataract model in vitro. *Exp. Eye Res.* 54, 73–81.
- Yelinova, V., Glazachev, Y., Khramtsov, V., Kudryashova, L., Rykova, V., Salganik, R.I., 1996. Studies of human and rat blood under oxidative stress: changes in plasma thiol level, antioxidant enzyme activity, protein carbonyl content, and fluidity of erythrocyte membranes. *Biochem. Biophys. Res. Commun.* 221, 300–303.